The Propagation of Ultrasonic Waves Through a Bubbly Liquid into Tissue: A Linear Analysis

by Quan Qi*, William D. O'Brien Jr.** and John G. Harris*

*Department of Theoretical and Applied Mechanics
216 Talbot Lab. 104 S. Wright St.
University of Illinois, Urbana, IL 61801

**Department of Electrical and Computer Engineering
1406 W. Green Street
University of Illinois, Urbana, IL 61801

Abstract

The steady state response induced by a harmonically driven, ultrasonic wave in a structure comprised of two layers, the first a bubbly liquid, and the second a viscoelastic solid with a rigid boundary, is studied in the linear approximation. This structure is intended to model a cavitating liquid in contact with tissue. The upper surface of the liquid is driven harmonically and models the source. The lower surface of the solid is rigid and models the bone. While cavitation is inherently nonlinear, the propagation process is approximated as linear. The transient response is not calculated. The model of the bubbly liquid is a simple continuum one, supplemented by allowing for a distribution of different equilibrium bubble radii and for the damping of the oscillations of each bubble. The model contains three functions, the probability distribution describing the distribution of bubble radii, and two functions modeling the mechanical response of the individual bubble and the tissue, respectively. Numerical examples are worked out by adapting data taken from various published sources to deduce the parameters of these functions. These examples permit an assessment of the overall attenuation of the structure, and of the magnitudes of the pressure and particle velocity in the bubbly liquid and of the traction and the particle displacement in the tissue.

1 Introduction

Our current understanding of ultrasonic cleaning is that collapsing bubbles with their concurrent jet formation at a surface are largely responsible for cleaning at relatively low frequencies. A single bubble has been shown (Plesset and Prosperetti 1977) to form a jet during collapse near a rigid surface where the jet is directed towards the surface. In the case of a compliant boundary, jet formation and its direction depend on the mechanical properties of the boundary and the adjacent liquid (Gibson and Blake 1982, Shima et al 1989, Duncan and Zhang 1991, Lush et al. 1992). Furthermore, it has been shown that a collection of gas bubbles may generate an order of magnitude larger pressure in a space without boundaries than that of a single bubble (Chahine 1982), suggesting that such collective behavior is important at surfaces as well. Because of the complicated nature of this problem, the interaction of ultrasound with a compliant boundary in a bubbly liquid is not well understood.

Wijngaarden (1968, 1972) developed a simple continuum model of the mechanical response of a liquid filled with bubbles (a bubbly liquid) in which the bubbles, which behave as oscillators, rather than the liquid itself, provide the compressibility. With this model he calculated the dispersion caused by the bubbles. Using a more complete linear model, that contains the effects of liquid compressibility and bubble-size distribution, Commander and Prosperetti (1989) also studied linear propagation in a bubbly liquid finding satisfactory agreement between their theory and experiments done by others. An approximate attempt to study a driven acoustic wavefield in a bubbly liquid confined by a transducer and a rigid plane was made by Hanson et al. (1982). We use a linearization of Wijngaarden's theory to model the liquid layer supplemented by a relation taken from Commander and Prosperetti that permits the bubble radii to vary, and by a heuristic relation that takes approximate account of the bubble damping. We model the tissue using a linear viscoelastic model suggested by Dinnar (1970), though we modify it slightly to make it regular for large time.

Ultrasonic devices designed to clean the surface of the skin are being used (HYDROSOUND(R), Arjo, Inc., Morton Grove, IL) thought little is known about what happens at the interface, as we indicated previously. Our goal here is to study the propagation of ultrasonic waves through a bubbly liquid into tissue. While we recognize that a linear model does not give a complete description of the cleaning, we anticipate that it will help us to understand the propagation processes, indicate, to an order of magnitude, the pressure and particle velocity throughout the structure and form a first step towards more complete modeling. Moreover, though this structure has a rich transient response we shall confine our study to the steady state response, because it is the most relevant to the application of interest.

2 Formulation

Governing Equations

INSERT Figure 1

In Fig. 1 we show the skin surface at $x = 0$, a driving transducer at $x = h$ and the bone at $x = -d$. The bubbly liquid is confined between the deformable tissue surface and the transducer, while between the tissue surface and the bone lie the epidermis, dermis and subcutaneous fat. The driving frequency of the transducer is of the order of 30 kHz so that the wavelength λ_g inside the bubble is approximately 11.3 mm. If we assume that the bubble radius R_0 is of the order of $0.5\mu m$ to $5\mu m$, the wavelength λ_g is larger than the bubble radius. Further, for air bubbles, the thermal penetration depth $l_{th} = (D_g/R_0\omega_0) \approx 20\mu m$, where D_g is the thermal diffusivity and ω_0 is the driving frequency, is a bit larger than the bubble radius. Accordingly, the inequalities $R_0 < l_{th} < \lambda_g$ are approximately satisfied, though the first may not always be true. Consequently (Wijngaarden 1972) we shall assume that the isothermal condition inside the bubble is approximately satisfied.

Dimensionless Linear Governing Equations

We shall work with linear approximations to the equations of motion written in terms of dimensionless variables. This is achieved by using the following,

$$\begin{aligned} R &= R_0(1+\varepsilon\hat{R}_1), \qquad \rho = \rho_0(1-\beta_0)(1+\varepsilon\hat{\rho}_1), \\ v &= \varepsilon v_0\hat{v}_1, \qquad p = p_0(1+\varepsilon\hat{p}_1), \qquad u = \varepsilon\omega_0^{-1}v_0\hat{u}_1, \\ \sigma &= p_0\varepsilon\hat{\sigma}_1, \qquad t = \hat{t}_1/\omega_0, \qquad x = \hat{x}_1 h, \\ J_T(t) &= J_T(0)\hat{J}_{T1} \quad and \quad J_B(t) = J_B(0)\hat{J}_{B1}, \end{aligned} \tag{1}$$

where $\varepsilon < 1$ is a small parameter characterizing the amplitude of the excitation, εv_0 is the particle velocity at the transducer's surface, and ω_0 is the driving frequency of the source. The dimensionless space and time variables are $\hat{x}_1$ and $\hat{t}_1$. The remaining symbols will be defined as they appear. We shall usually drop the ^ when there is no possibility of confusion, but retain the subscript 1.

The following are the dimensionless linear governing equations for the bubbly liquid between $1 \geq x_1 \geq 0$.

$$\frac{\partial \rho_1}{\partial t_1} + \frac{v_0}{\omega_0 h}\frac{\partial v_1}{\partial x_1} = 0 \ , \tag{2}$$

$$\frac{\partial v_1}{\partial t_1} + \frac{p_0}{\rho_0(1-\beta_0)v_0\omega_0 h}\frac{\partial p_1}{\partial x_1} = 0 \ , \tag{3}$$

and

$$\rho_1 = -\frac{4\pi}{1-\beta_0}\int_0^\infty R_0^3 \ R_1(R_0;t_1,x_1) \ f(R_0,x_1)\,dR_0. \tag{4}$$

Equation (2) is the linearized mass conservation, Eq. (3) is the momentum conservation, and Eq. (4), suggested by Commander and Prosperetti (1989), is obtained from a relation between density and volume fraction. The terms ρ_1, v_1 and p_1 are the dimensionless perturbations in density, particle velocity and pressure. The terms ρ_0 and p_0 are the corre-

sponding equilibrium density and pressure. The function $f(R_0, x_1)$ is a distribution function for the bubble radii whose unperturbed radii are R_0. The term R_1 is the dimensionless perturbation to the bubble radius. The number of bubbles per unit volume with equilibrium radius between R_0 and $R_0 + dR_0$ is given by $dN = f(R_0, x_1)\, dR_0$ and the equilibrium volume fraction is given by,

$$\beta_0 = \frac{4\pi}{3}\int_0^\infty R_0^3 f(R_0; x_1)\, dR_0. \tag{5}$$

In general, R_1 depends on the corresponding equilibrium radius R_0, as well as on x_1 and t_1. Note that, while some bubbles may be forming or collapsing, we are assuming that there is, on average, a large collection of bubbles already existing in the liquid. In part, this is why we shall not consider the transient motion.

For the tissue between $0 > x_1 > -d/h$ the governing equations are

$$\frac{\partial^2 u_1}{\partial t_1^2} = \frac{p_0}{\rho_s h v_0 \omega_0}\frac{\partial \sigma_1}{\partial x_1}, \tag{6}$$

$$\frac{\partial u_1}{\partial x_1} = \frac{\omega_0 p_0 h J_T(0)}{v_0}\left[\int_{0^-}^{t_1} J_{T1}(t_1 - \tau)\frac{\partial \sigma_1}{\partial \tau}\, d\tau\right]. \tag{7}$$

The terms u_1 and σ_1 are the dimensionless perturbations in particle displacement and normal traction. The term ρ_s is the average unperturbed tissue density. The function J_{T1} is the creep compliance and $J_T(0)$ is its initial value. Equation (6) is the momentum conservation and Eq. (7) is the constitutive relation for the tissue. A dimensionless form of J_{T1} is given in the discussion section.

It remains to complete the model for the bubbly liquid. By analogy with the model for the tissue we include damping in the linearized Rayleigh-Plesset equation as follows.

$$\frac{\partial^2 R_1}{\partial t_1^2} + \Omega^2 R_1 = -\frac{p_0}{\rho_0 R_0^2 \omega_0^2} p_1 + \frac{J_B(0)}{\rho_0 R_0^2 \omega_0^2} \int_0^{t_1} J_{B1}(t_1 - \tau) \frac{\partial R_1}{\partial \tau} d\tau \tag{8}$$

The function J_{B1} describes the damping of the bubble oscillations and $J_B(0)$ is its initial value. It enters the linearized Rayleigh-Plesset equation in a way analogous to that in which the creep compliance enters the equations describing the tissue. We shall approximate J_{B1} in the frequency domain in ways that emulate damping mechanisms determined from experiments or more accurate models. Note that by taking J_{B1} to be a delta function the usual viscous damping is recovered. When deriving Eq. (8) the static relation $p_{g0} = p_0 + 2\Gamma/R_0$ has been used. The dimensionless natural frequency Ω is given by

$$\Omega^2 = \frac{1}{\rho_0 (R_0 \omega_0)^2} \left[3p_{g0} - \frac{2\Gamma}{R_0} \right], \tag{9}$$

where Γ denotes the surface tension coefficient and p_{g0} is the equilibrium pressure in the bubble. For completeness, the original nonlinear governing equations for the bubbly liquid, from which Eqs. (2)-(5) and Eq. (8) are derived, are summarized in Appendix A. The creep compliance for the nonlinear governing equations for the tissue is not known, so that, in that case, we started from the linear equations.

Finally, the corresponding dimensionless boundary and continuity conditions are

$$v_1 = H(t_1) e^{it_1}, \qquad x_1 = 1, \tag{10}$$

$$v_1 = \frac{\partial u_1}{\partial t_1}, \qquad \sigma_1 = -p_1, \qquad x_1 = 0, \tag{11}$$

and

$$u_1 = 0, \qquad x = -\frac{d}{h}. \tag{12}$$

3 Solutions

Though we have formulated the problem in the time domain we shall be concerned only with the steady state response. We could, of course, have begun by working in the frequency domain, but, because the creep compliance J_{T1} is known in the time domain we began there. To map to the frequency domain we use the following Fourier transform pair.

$$\bar{f}(\omega) = \frac{1}{(2\pi)^{1/2}} \int_{-\infty}^{\infty} f(t_1)\, e^{-i\omega t_1} dt_1, \qquad f(t_1) = \frac{1}{(2\pi)^{1/2}} \int_{-\infty}^{\infty} \bar{f}(\omega)\, e^{i\omega t_1} d\omega. \tag{13}$$

Note that for $f(t_1)$ to be 0 for $t_1 < 0$, $\bar{f}(\omega)$ must be analytic throughout the $Im(\omega) < 0$ plane. The transformed terms are given by the previously defined symbols but have an overbar. The argument ω may also be indicated. Equations (2) to (4) and (8) become

$$\frac{d}{dx_1}\bar{v}_1(\omega, x_1) = -i\omega \frac{h\omega_0}{v_0} \bar{\rho}_1(\omega, x_1), \tag{14}$$

$$\frac{d}{dx_1}\bar{p}_1(\omega, x_1) = -i\omega \frac{\rho_0 (1-\beta_0) v_0 \omega_0 h}{p_0} \bar{v}_1(\omega, x_1), \tag{15}$$

$$\bar{\rho}_1(\omega, x_1) = -\frac{4\pi}{1-\beta_0} \int_0^{\infty} R_0^3\ \bar{R}_1(R_0; \omega, x_1)\ f(R_0, x_1)\, dR_0, \tag{16}$$

and

$$\bar{p}_1(\omega, x_1) = \frac{\rho_0 R_0^2 \omega_0^2}{p_0} \left[\omega^2 - \Omega^2 + \frac{i\omega (2\pi)^{1/2} J_B(0)\, \bar{J}_{B1}(\omega)}{\rho_0 R_0^2 \omega_0^2} \right] \bar{R}_1(R_0; \omega, x_1). \tag{17}$$

Moreover, Eqs. (6) and (7) become

$$\frac{d}{dx_1}\bar{\sigma}_1(\omega, x_1) = -\frac{\rho_s h v_0 \omega_0}{p_0} \omega^2 \bar{u}_1(\omega, x_1), \tag{18}$$

and

$$\frac{d}{dx_1}\bar{u}_1(\omega, x_1) = \frac{(2\pi)^{1/2} p_0 h J_T(0)\, \omega_0}{v_0} \bar{\sigma}_1(\omega, x_1)\, \omega i \bar{J}_{T1}(\omega), \tag{19}$$

The transformed creep compliance is described in the discussion section. Finally, the transformed boundary and continuity conditions, Eqs. (10) to (12), become

$$\bar{v}_1(\omega, 1) = \frac{1}{i(\omega - 1)\sqrt{2\pi}}, \tag{20}$$

$$\bar{v}_1(\omega, 0) = i\omega\bar{u}_1(\omega, 0), \; \bar{\sigma}_1(\omega, 0) = -\bar{p}_1(\omega, 0) \tag{21}$$

and

$$\bar{u}_1(\omega, -d/h) = 0. \tag{22}$$

Note that the contour for the inverse transform will pass below the pole at $\omega = 1$.

Equations (14) to (17) may be combined to give

$$\frac{d}{dx_1}\begin{bmatrix}\bar{p}_1 \\ \bar{v}_1\end{bmatrix} + i\omega\begin{bmatrix}0 & a_1 \\ a_2 & 0\end{bmatrix}\begin{bmatrix}\bar{p}_1 \\ \bar{v}_1\end{bmatrix} = 0, \tag{23}$$

where

$$a_1 = \frac{\rho_0 v_0 \omega_0 h(1 - \beta_0)}{p_0}, \tag{24}$$

$$a_2 = \left(\frac{4\pi}{1 - \beta_0}\right)\frac{p_0\omega_0 h}{\rho_0 v_0}\int_0^\infty \frac{R_0^3 f(R_0, x_1)\, dR_0}{\left[3\beta_0 c_0^2 - \omega^2\omega_0^2 R_0^2 - i\omega(2\pi)^{1/2}\omega_0^2 R_0^2 J_B(0)\bar{J}_{B1}/\rho_0\right]} \tag{25}$$

and

$$c_0^2 = \frac{p_{g0}}{\rho_0\beta_0} - \frac{2\Gamma}{3\beta_0\rho_0 R_0} = \frac{(R_0\omega_0)^2}{3\beta_0}\Omega^2. \tag{26}$$

The term c_0 is the sound speed in a bubbly liquid having a uniform equilibrium bubble radius R_0 (Hsieh 1988). The solution to Eq. (23) is

$$\begin{bmatrix}\bar{p}_1 \\ \bar{v}_1\end{bmatrix} = \begin{bmatrix}-\sqrt{a_1/a_2}\{iA_0\sin\bar{\lambda}x_1 + B_0\cos\bar{\lambda}x_1\} \\ A_0\cos\bar{\lambda}x_1 + iB_0\sin\bar{\lambda}x_1\end{bmatrix} \tag{27}$$

where $\bar{\lambda} = \sqrt{a_1 a_2}\omega$, and A_0 and B_0 are constants of integration. Similarly, Eqs. (18) and (19) may be combined to give

$$\frac{d}{dx_1}\begin{bmatrix} \bar{\sigma}_1 \\ i\omega\bar{u}_1 \end{bmatrix} + i\omega\begin{bmatrix} 0 & b_1 \\ b_2 & 0 \end{bmatrix}\begin{bmatrix} \bar{\sigma}_1 \\ i\omega\bar{u}_1 \end{bmatrix} = 0, \tag{28}$$

where

$$b_1 = -\rho_s \frac{h v_0 \omega_0}{p_0} \tag{29}$$

and

$$b_2 = -\frac{(2\pi)^{1/2} h\omega_0 p_0 J_T(0)}{v_0} i\omega \bar{J}_{T1}(\omega). \tag{30}$$

As with Eq. (23) the solution to Eq. (28) is

$$\begin{bmatrix} \bar{\sigma}_1 \\ \bar{u}_1 \end{bmatrix} = \begin{bmatrix} -\sqrt{b_1/b_2}\{iC_0 \sin\hat{\lambda}x_1 + D_0 \cos\hat{\lambda}x_1\} \\ \{C_0 \cos\hat{\lambda}x_1 + iD_0 \sin\hat{\lambda}x_1\} \end{bmatrix}, \tag{31}$$

where $\hat{\lambda} = \sqrt{b_1 b_2}\omega$, and C_0 and D_0 are constants of integration.

Applying the boundary and continuity conditions, we find,

$$\bar{p}_1 = -\sqrt{\frac{a_1}{a_2}} \frac{\sin\hat{\lambda}\frac{d}{h}\sin\bar{\lambda}x_1 + \sqrt{\frac{a_2 b_1}{a_1 b_2}}\cos\hat{\lambda}\frac{d}{h}\cos\bar{\lambda}x_1}{\sin\hat{\lambda}\frac{d}{h}\cos\bar{\lambda} - \sqrt{\frac{a_2 b_1}{a_1 b_2}}\cos\hat{\lambda}\frac{d}{h}\sin\bar{\lambda}} \frac{1}{(\omega - 1)\sqrt{2\pi}}, \tag{32}$$

$$\bar{v}_1 = \frac{\sin\hat{\lambda}\frac{d}{h}\cos\bar{\lambda}x_1 - \sqrt{\frac{a_2 b_1}{a_1 b_2}}\cos\hat{\lambda}\frac{d}{h}\sin\bar{\lambda}x_1}{\sin\hat{\lambda}\frac{d}{h}\cos\bar{\lambda} - \sqrt{\frac{a_2 b_1}{a_1 b_2}}\cos\hat{\lambda}\frac{d}{h}\sin\bar{\lambda}} \frac{1}{(\omega - 1)\, i\sqrt{2\pi}}, \tag{33}$$

$$\bar{\sigma}_1 = \sqrt{\frac{b_1}{b_2}} \frac{\cos\hat{\lambda}\,(x_1 + \frac{d}{h})}{\sin\hat{\lambda}\frac{d}{h}\cos\bar{\lambda} - \sqrt{\frac{a_2 b_1}{a_1 b_2}}\cos\hat{\lambda}\frac{d}{h}\sin\bar{\lambda}} \frac{1}{(\omega - 1)\sqrt{2\pi}}, \tag{34}$$

and

$$i\omega\bar{u}_1 = \frac{\sin\hat{\lambda}\,(x_1 + \frac{d}{h})}{\sin\hat{\lambda}\frac{d}{h}\cos\bar{\lambda} - \sqrt{\frac{a_2 b_1}{a_1 b_2}}\cos\hat{\lambda}\frac{d}{h}\sin\bar{\lambda}} \frac{1}{(\omega - 1)\, i\sqrt{2\pi}}. \tag{35}$$

4 Discussion

Bubble size distribution

Before calculating the steady state response arising from the pole at $\omega = 1$, two simple cases of equilibrium bubble size distributions are noted. For a uniform distribution of equilibrium bubble radii $\bar{R}_0$, we have,

$$f(R_0, x_1) = N\delta\,(R_0 - \bar{R}_0)\,, \tag{36}$$

where N is the number of bubbles per unit volume. Correspondingly, we find that

$$a_2 = \frac{3\beta_0}{1-\beta_0}\frac{p_0\omega_0 h}{\rho_0 v_0}\frac{1}{[3\beta_0 c_0^2 - \omega^2\omega_0^2 R_0^2 - i\omega\,(2\pi)^{1/2} J_B\,(0)\,\bar{J}_{B1}/\rho_0]}, \tag{37}$$

where $\beta_0 = 4\pi\bar{R}_0^{\,3} N/3$. For a discrete distribution of equilibrium radii $\bar{R}_{0j}$, $j = 1, 2, \ldots,$

$$f(R_0, x_1) = \sum_j N_j \delta\,(R_0 - \bar{R}_{0j}) \tag{38}$$

and

$$a_2 = \frac{4\pi}{1-\beta_0}\frac{p_0\omega_0 h}{\rho_0 v_0}\sum_j \frac{N_j \bar{R}_{0j}^3}{\left[3\beta_0 c_{0j}^2 - \omega^2\omega_0^2\bar{R}_{0j}^2 - i\omega\,(2\pi)^{1/2} J_{Bj}\,(0)\,\bar{J}_{B1j}/\rho_0\right]}, \tag{39}$$

where c_{0j} is given by Eq. (26) with R_0 replaced by $\bar{R}_{0j}$ and β_0 is a sum over j. There may be a dependence of J_B on R_0, hence we have placed a subscript j on $J_{Bj}(0)$ and $\bar{J}_{B1j}$. More complicated distributions can also be handled with Eq. (25) once the appropriate distribution function is specified.

Attenuation in the tissue

The dimensionless form of J_{T1} is given by

$$J_{T1}(t_1) = \left\{ \frac{J_T(\infty)}{J_T(0)} + e^{-\frac{\lambda}{\omega_0} t_1} \left[1 - \frac{J_T(\infty)}{J_T(0)} + \frac{t_1}{J_T(0)\,\omega_0 Q_1} \right] \right\} H(t_1), \tag{40}$$

where $\lambda = Q_1/Q_2$ and $J_T(0) = P_2/Q_2$, and $J_T(\infty) = (P_1 Q_1 - Q_2)/Q_1^2$. The Q_i and P_i are obtained from measurements. The function $H(t_1)$ is the Heaviside function. Typical values of Q_i and P_i for tissue are (Dinnar 1970 and Nyborg 1975)

$Q_1 = 10^4$	$Q_2 = 1.8 \times 10^2$	$P_1 = 6.8 \times 10^{-2}$	$P_2 = 0.72 \times 10^{-3}$
$(\dot{N}s/m^2)$	(Ns^2/m^2)	(s)	(s^2)

In contrast to Dinnar we modify J_{T1} slightly to make it regular at large time. Note that its small time behavior is not changed. The transformed creep compliance is given by (Lighthill 1970)

$$\bar{J}_{T1}(\omega) = \frac{J_T(\infty)}{J_T(0)} \left[\frac{1}{\sqrt{2\pi} i\omega} \right] + \left(1 - \frac{J_T(\infty)}{J_T(0)} \right) \frac{1}{\sqrt{2\pi}} \frac{1}{i\omega + \lambda/\omega_0} - \frac{1}{\sqrt{2\pi}\,\omega_0 Q_1 J_T(0)} \frac{1}{(\omega - i\lambda/\omega_0)^2} \tag{41}$$

Note that the inversion contour will pass below the pole at $\omega = 0$. Moreover, we can show that $[i\omega \bar{J}_{T1}(\omega)]^{1/2}$ has two unequal branch points located on the imaginary axis and a simple pole at $i\lambda/\omega_0$.

Attenuation in the bubbly liquid

In Eq. (8) we heuristically added damping into the equation for the bubble oscillations. While $J_B(t) = J_B(0) J_{B1}(t)$ is arbitrary, it must be real and $J_B(t) = 0$ for $t < 0$. This implies that $\bar{J}_B^*(-\omega) = \bar{J}_B(\omega)$, where $\bar{J}_B^*$ is the complex conjugate, and $\bar{J}_B(\omega)$ must be analytic in the $Im(\omega) < 0$ plane. In what follows we shall approximate $\bar{J}_B(\omega)$ for ω real and positive, with the understanding that the function would have to be continued in such a way as to satisfy these general criteria if we wished to recover an appropriate $J_B(t)$.

An approximate expression for $\bar{J}_{B1}$ can be obtained by comparing with results given in Commander and Prosperetti (1989). That comparison gives,

$$\bar{J}_{B1} = -2\frac{\rho_0 \bar{R}_0^2 \omega_0}{J_B(0)}\left[\frac{2\mu}{\rho_0 \bar{R}_0^2} + \frac{p_{g0}}{2\rho_0 \omega_0 \bar{R}_0^2} Im\Phi\right], \qquad (42)$$
$$+ \frac{p_{g0}}{i\omega J_B(0)}(3 - Re\Phi)$$

where μ is the viscosity of the fluid. The two real terms represent attenuation due to viscosity and heat transfer. Furthermore, we have

$$\Phi = \frac{3\gamma}{1 - 2(\gamma - 1) i\chi [(i/\chi)^{1/2} \coth (i/\chi)^{1/2} - 1]}, \qquad (43)$$

where γ is the ratio of the specific heat in the bubble, $\chi = D_g / (\omega_0 \bar{R}_0^2)$, and D_g is the gas thermal diffusivity. It has been indicated (Wijngaarden 1972), however, that the attenuation of a bubble oscillation with an equilibrium radius $\bar{R}_0$ of the order of $0.5–5\mu m$ is primarily thermal. Moreover, it is suggested (Wijngaarden 1972) that the following simple expression can be used for this range of bubble radii,

$$\bar{J}_{B1} = -\frac{\rho_0 \bar{R}_0^2 \omega_0 \omega_b}{(2\pi)^{1/2} J_B(0)} \delta_{th} = -4.45 \times 10^{-4} \frac{\rho_0 \bar{R}_0^2 \omega_0^{1/2} \omega_b^2}{2\pi J_B(0)}. \tag{44}$$

A numerical comparison shows that the value of $\bar{J}_{B1}$ estimated by Eq. (42) is of the same order of magnitude as that predicted by Eq. (44). Therefore, we shall use Eq. (44) for our numerical examples. Note that $\bar{J}_{B1j}$ is given by Eq. (44) with $\bar{R}_0$ replaced by $\bar{R}_{0j}$.

Although we have used the isothermal assumption and neglected heat transfer and the compressibility of the liquid at the outset, their contribution to overall attenuation can be heuristically included by choosing the appropriate form of $\bar{J}_{B1}$. Such an approach is consistent with the available model for the tissue's constitutive relation.

By analogy with a propagating plane wave, the following expression is found for the attenuation coefficient per unit length D is found to be

$$D = 8.69 \left[\frac{2 \times 4.45 \times 10^{-4}}{3(2\pi)^{1/2}} \frac{\omega_0^{3/2}}{c^3} (\bar{R}_0 \omega_b)^2 \right] \quad (dB/m)$$

where c is the sound speed in the liquid without bubbles. For $\omega_0 = 60000\pi\,(r/s)$, we find

$$D = (0.02, 0.68, 0.74) \quad (dB/cm) \text{ for } \bar{R}_0 = (0.5, 5, 50) \quad (\mu m) \text{ respectively.}$$

These results compare favorably with the experiments by O'Brien and Smith (1994) in which it was found that

$$D \sim 0.43 \quad (dB/cm).$$

One might infer from the comparison that the equilibrium radii probably fall within the range of $0.5 \sim 5 \quad (\mu m)$.

INSERT Figure 2

Steady state solutions

Because $t_1 > 0$, the inversion contour must be closed in the $Im\,(\omega) > 0$ half plane. Recalling the expressions for $\hat{\lambda}$, $\bar{\lambda}$, a_1, a_2, b_1 and b_2, we see that possible branch points and poles come from $a_2 \to \infty$ and $b_2 = 0$, or, using Eq. (39),

$$3\beta_0 c_{0j}^2 - \omega^2 \omega_0^2 \bar{R}_{0j}^2 - i\omega (2\pi)^{1/2} J_{Bj}(0)\, \bar{J}_{B1j}(\omega)/\rho_0 = 0 \tag{45}$$

and

$$i\omega \bar{J}_{T1}(\omega) = 0. \tag{46}$$

These points and any poles that arise from the common factor in the denominator of Eqs. (32) to (35) are in the $Im\,(\omega) > 0$ half plane, correspond to the transient solutions and will be damped out leaving the steady state response from the pole at $\omega = 1$. The structure of the complex ω plane is sketched in Fig. 2. Note that though $\bar{J}_{B1}$ appears to have a branch point at $\omega = 0$, a more accurate estimate of $\bar{J}_{B1}$ would move the branch point into $Im\,(\omega) > 0$ half plane. We have indicated the branch cuts associated with $\bar{J}_{B1}$. Moreover, note that if there were no layering, the branch cuts would still be present indicating that the bubbly liquid and the solid are dispersive. The additional poles indicate the resonances caused by the layering.

The steady state solutions are,

$$p_1 = -\left\{ \sqrt{\frac{a_1}{a_2}} \frac{\sin\hat{\lambda}\frac{d}{h}\sin\bar{\lambda}x_1 + \sqrt{\frac{a_2 b_1}{a_1 b_2}}\cos\hat{\lambda}\frac{d}{h}\cos\bar{\lambda}x_1}{\sin\hat{\lambda}\frac{d}{h}\cos\bar{\lambda} - \sqrt{\frac{a_2 b_1}{a_1 b_2}}\cos\hat{\lambda}\frac{d}{h}\sin\bar{\lambda}} \right\}\Bigg|_{\omega=1} ie^{it_1}, \tag{47}$$

$$v_1 = \left\{ \frac{\sin\hat{\lambda}\frac{d}{h}\cos\bar{\lambda}x_1 - \sqrt{\frac{a_2 b_1}{a_1 b_2}}\cos\hat{\lambda}\frac{d}{h}\sin\bar{\lambda}x_1}{\sin\hat{\lambda}\frac{d}{h}\cos\bar{\lambda} - \sqrt{\frac{a_2 b_1}{a_1 b_2}}\cos\hat{\lambda}\frac{d}{h}\sin\bar{\lambda}} \right\}\Bigg|_{\omega=1} e^{it_1}, \tag{48}$$

$$\sigma_1 = \left\{ \sqrt{\frac{b_1}{b_2}} \frac{\cos\hat{\lambda}\,(x_1 + \frac{d}{\bar{h}})}{\sin\hat{\lambda}\frac{d}{\bar{h}}\cos\bar{\lambda} - \sqrt{\frac{a_2 b_1}{a_1 b_2}}\cos\hat{\lambda}\frac{d}{\bar{h}}\sin\bar{\lambda}} \right\}\Bigg|_{\omega = 1} ie^{it_1}, \tag{49}$$

and

$$iu_1 = \left\{ \frac{\sin\hat{\lambda}\,(x_1 + \frac{d}{\bar{h}})}{\sin\hat{\lambda}\frac{d}{\bar{h}}\cos\bar{\lambda} - \sqrt{\frac{a_2 b_1}{a_1 b_2}}\cos\hat{\lambda}\frac{d}{\bar{h}}\sin\bar{\lambda}} \right\}\Bigg|_{\omega = 1} e^{it_1}, \tag{50}$$

where because $t_1 \geq 0$ the step function proceeding each solution has been dropped.

Bubble resonance: $a_2 \to \infty$

From Eq. (39) the bubble resonance occurs for

$$c_{0j}^2 - \frac{\omega^2\omega_0^2}{3\beta_0}\bar{R}_{0j}^2 - i\omega\frac{\sqrt{2\pi}J_{Bj}(0)\,\bar{J}_{B1j}(\omega)}{3\beta_0\rho_0} = 0, j = 1, 2, \ldots \tag{51}$$

where subscript j is kept to denote a possible discrete distribution of equilibrium bubble sizes. Therefore, when $\bar{J}_{B1j} = 0$ this limit is equivalent to

$$\omega^2\omega_0^2 \to \left(\frac{3p_{g0}}{\rho_0} - \frac{2\Gamma}{\rho_0\bar{R}_{0j}}\right)\frac{1}{\bar{R}_{0j}^2} = \omega_0^2\Omega_j^2 \equiv \omega_{bj}^2, j = 1, 2, \ldots \tag{52}$$

From Plesset and Prosperetti (1977), ω_{bj} is the natural frequency for the oscillation of a single bubble with equilibrium radius $\bar{R}_{0j}$. Consequently, for this case $\omega = 1$ corresponds to driving the bubbly liquid at one of the bubble resonant frequencies.

Note that the right hand sides of Eqs. (47) to (50) at $\omega = 1$ are indeterminate in this case. These indeterminate solutions may be explained as a consequence of an increase in the scattering cross section (Commander and Prosperetti 1989) in the neighborhood of the bubble resonant frequency. Most of the input energy is being scattered by resonant bubbles

at the surface of the transducer and little is left to penetrate the bubbly liquid and be delivered to the tissue surface.

As a normal operational procedure, the liquid used with HYDROSOUND(R) (Arjo, Inc. Morton Grove, IL) is usually treated so that large bubbles are eliminated allowing the ultrasonic waves to penetrate the liquid. Furthermore, this partial degassing also helps to suppress rectified diffusion preventing the growth of small bubbles to resonant size. In the numerical examples to be worked out, one of the equilibrium bubble radii is taken to be $5\mu m$. Such a size seems appropriate for a bubbly liquid in which the initial cavitation events have died away and a steady state has been established.

Numerical examples

Using the values for the P_i and the Q_i given below Eq. (40), we obtain,

$$\begin{aligned} J_T(0) &= P_2/Q_2 = 4\times 10^{-6}\,(m^2/N) \\ J_T(\infty) &= 5\times 10^{-6}\,(m^2/N) \end{aligned} \tag{53}$$

and

$$\lambda = Q_1/Q_2 = 5.56\times 10 \quad (1/s)\,. \tag{54}$$

From these we find that

$$\sqrt{2\pi i}\bar{J}_{T1}(1) \approx 1 - 2.07\times 10^{-4} i. \tag{55}$$

The intensity of the acoustic wavefield is taken to be $I = 1200 \quad (W/m^2)$ (characteristic of a skin cleaning operation) so that $v_0 = 4 \quad (m/s)$ and $\varepsilon = 0.01$. Furthermore, we assume that $d = 1\,(mm)$, $h = 10 \quad (cm)$, $\rho_s = 1100\,(kg/m^3)$, $\rho_0 = 1000\,(kg/m^3)$, and $\beta_0 = 10^{-4}$. The ambient pressure is assumed to be atmospheric, i.e. $p_0 = 10^5\,(Pa)$ and the surface tension coefficient is taken to be $\Gamma = 0.073\,(Pa/m)$. We choose the driving frequency and the equilibrium bubble radius as variable parameters. However, we shall assume that there is only a single bubble radius for each case.

INSERT Figure 3

Figure 3 gives the magnitudes of (a) the acoustic pressure $|p_1|$ and (b) the particle velocity $|v_1|$ in the bubbly liquid for a driving frequency $f_0 = 30kHz$ and three different equilibrium bubble radii $\bar{R}_0 = 0.5, 5$ and $50\mu m$. The amplitude of the spatial oscillation decreases with the increase of equilibrium bubble radii and the spatial periodicity is also affected by the variation of $\bar{R}_0$.The pressure and velocity amplitudes associated with $R_0 = 50\mu m$ are negligible.

INSERT Figure 4

Figure 4 gives the magnitude of (a) the normal component of traction $|\sigma_1|$ and (b) the displacement in the tissue $|u_1|$ for the same driving frequency $f_0 = 30kHz$ and equilibrium bubble radii $\bar{R}_0 = 0.5$ and $5\mu m$. In contrast to case of the bubbly liquid, the spatial periodicity is not affected by the variation of $\bar{R}_0$. The amplitude of the spatial oscillation decreases with the increase of equilibrium bubble radii. There is no appreciable spatial attenuation in the tissue because of its low attenuation.

INSERT Figure 5

Figure 5 gives the magnitudes of (a) the acoustic pressure $|p_1|$ and (b) the particle velocity $|v_1|$ in the bubbly liquid for an equilibrium bubble radii $\bar{R}_0 = 5\mu m$ and three different driving frequencies $f_0 = 19, 30$ and $41kHz$. Higher driving frequencies lead to more significant spatial attenuation. While velocity at the tissue surface decreases with increasing driving frequency, the pressure at the tissue surface remains more or less constant.

INSERT Figure 6.

A non-monotonic amplitude variation of both normal component of traction $|\sigma_1|$ and displacement $|u_1|$ in the tissue can be observed from Fig. 6. Here, $f_0 = 30kHz$ is seen to excite the largest response in the tissue and $f_0 = 41kHz$ leads to the smallest. This happens because the finite thicknesses of the bubbly liquid and tissue layers introduce a set of natural frequencies. In fact, the denominator in Eqs. (47) to (50) can be shown to have a zero near $f = 30kHz = \omega/2\pi$ if the attenuation in both the bubbly liquid and the tissue layer are small. This zero corresponds to one of the poles denoting the natural frequencies of the structure and is indicated in Fig. 2.

Finally, the resonant bubble frequencies are found to be $f_b = 9 \times 10^2$, 5.24×10^2 and $54.8\ kHz$ for $\bar{R}_0 = 0.5$, 5 and $50\mu m$, respectively. Clearly, all are above the driving frequencies used in the numerical calculations. Also, corresponding to a driving frequency of $30kHz$, the resonant bubble radius is found to be $92.2\mu m$.

5 Concluding remarks

A linear model for propagation in a layered structure comprising a bubbly liquid adjacent to a viscoelastic solid, that models tissue, has been proposed and explored. It depends upon three functions $f(R_0, x_1)$, $J_T(t_1)$ and $J_B(t_1)$ whose form can be estimated either from theory or measurement. It is clear that propagation will not take place efficiently unless the spectrum of resonant frequencies for the bubbles is avoided. The numerical results indicate the spatial distributions of pressure and velocity in the bubbly liquid, and traction and displacement in the tissue. Specifically, spatial attenuation is observed in the bubbly liquid and is more significant for higher driving frequencies. In contrast, little spatial attenuation is observed in the tissue. The layering introduces resonances, one or more of which can be excited.

6 Acknowledgment

Quan Qi thanks the manufacturing Research Center at UIUC, the Hunt family and the Acoustical Society of America for partial financial support. John G. Harris was partially supported by NSF, Grant No.MSS-9114547. William.D. O'Brien and Quan Qi were partially supported by the Arjo, Inc.

7 References

Chahine, G.L. 1982. "Pressure generated by a bubble cloud collapse," in *ASME Cavitation and Polyphase Flow Forum*, ed. Hoyt, J.W. ASME: New York, pp. 27-31.

Commander, K. W. and Prosperetti, A. 1989. "Linear pressure waves in bubbly liquids: comparison between theory and experiments," J. Acoust. Soc. Am. 85, pp. 732-746.

Dinnar U. 1970. "A note on the theory of deformation in compressed skin tissues", Mathematical Bioscience 8, pp. 71-82.

Duncan, J.H. and Zhang, S. 1991. "On the interaction of a collapsing cavity and a compliant wall", J. Fluid Mech. 226, pp.401-423.

Gibson, D.C. and Blake J.R. 1982. "The growth and collapse of bubbles near deformable surfaces" Appl. Sci. Res. 38, pp215-224.

Hanson, I, Kedrinskii, V and Morch, K.A. 1982. "On the dynamics of cavity clusters" J. Phys. D: Appl. Phys., 15, pp.1725-1735.

Hsieh, D.Y. 1988. "On dynamics of bubbly liquids", in *Advances in Applied Mechanics*, Vol. 26, ed. by Hutchinson, J.W and Wu, T.Y, pp. 63-133.

Lighthill, M. J. 1970. *Fourier Analysis and Generalized Functions,* The University Press, Cambridge, pp. 42-44.

Lush, P.A., Takayama, K. Tomita, T. and Obara, T. 1992. "Cavitation and induced shock wave-bubble interaction as a cause of human tissue damage in extracorporeal shockwave lithotripsy," in Proc. Inst. Mech. Engineers Cavitation, IMechE 1992-11. Mechanical Engineering Publication, London, pp. 55-63.

Nyborg, W. L. 1975. *Intermediate Biophysical Mechanics*, Cummings Publishing Company, Menlo Park, CA, pp. 216-219.

O'Brien, W.D. Jr. and Smith, N.B. 1994. Personal communication.

Plesset, M.S. and Prosperetti, A 1977. "Bubble dynamics and cavitation", Ann. Rev. Fluid Mech., Vol. 9, ed. Van Dyke, M., Wehausen, J.V. and Lumley, J.L., pp.145-185.

Shima, A, Tomita, Y, Gibson, D.C., and Blake, J.B. 1989. "The growth and collapse of cavitation bubbles near composite surface", J. Fluid Mech. 203, pp.199-214.

Wijngaarden, Van 1968. "On the equations of motion for mixtures of liquid and gas bubbles", J. Fluid Mech., 33, pp 465-474.

Wijngaarden, Van 1972. "One-dimensional flow of liquids containing small gas bubbles", Ann. Rev. Fluid Mech., Vol 4, ed. Van Dyke, M., Vincenti, W. G. and Wehausen, J.V., pp.369-390.

8 Appendix A: The nonlinear equations for the bubbly liquid

The fully nonlinear one-dimensional theory leads to the following governing equations for the liquid and gas bubble mixture (Wijngaarden 1968 and 1972).

$$\frac{\partial \rho}{\partial t} + \frac{\partial}{\partial x}(\rho v) = 0, \tag{A.1}$$

$$\rho \frac{\partial v}{\partial t} + \rho v \frac{\partial v}{\partial x} + \frac{\partial p}{\partial x} = 0, \tag{A.2}$$

$$\rho = \rho_0 [1 - \beta], \tag{A.3}$$

$$\rho_0 \left[R \frac{\partial^2 R}{\partial t^2} + \frac{3}{2} \left(\frac{\partial R}{\partial t}\right)^2 + \frac{2\Gamma}{\rho_0 R} \right] = p_g - p, \tag{A.4}$$

and

$$p_g = p_{g_0} \left(\frac{R_0}{R}\right)^3, \tag{A.5}$$

where Eq. (A.1) is the mass conservation for the bubbly liquid, Eq. (A.2) is the momentum conservation, Eq. (A.3) is a relation that expresses the density variation of the bubbly liquid in terms of varying bubble radii, and Eq. (A.4) is the Rayleigh-Plesset equation (Wijngaarden 1972 and Hsieh 1988). Note that the motion of the bubble is assumed to be spherically symmetric. The isothermal assumption Eq. (A.5) gives the pressure inside the bubble p_g in terms of its equilibrium value p_{g_0} and the bubble radius R whose initial value is R_0. The possibility of having different sized bubbles may be taken into account by setting (Commander and Prosperetti 1989)

$$\beta = \frac{4}{3}\pi \int_0^\infty R^3 (R_0; x, t) f(R_0, x)\, dR_0, \tag{A.6}$$

where $f(R_0, x)$ is a probability density function denoting the number of bubbles for a given equilibrium radius R_0 located at x.

In these equations, ρ, v and p are respectively the density, particle velocity and pressure of the mixture of liquid and gas bubbles. The gas density is considered negligible compared with that of the fluid ρ_0, β_0 is the initial gas volume fraction, and Γ is the surface tension. Following Wijngaarden (1972) and Hsieh (1988), the compressibility of the liquid is neglected. The inertia of the bubbly liquid is that of the liquid and the compressibility is provided by the gas bubbles. The concentration of gas is assumed small so that interactions and translational motion of the bubbles can be neglected.

Figure captions for "The propagation of ultrasonic waves through a bubbly liquid into tissue: a linear analysis" by Qi, O'Brien and Harris

Figure 1. The geometry of the problem. The origin is at the tissue surface.

Figure 2. A sketch of the complex ω plane.

Figure 3. The magnitude of (a) the acoustic pressure $|p_1|$ and (b) the particle velocity $|v_1|$ are plotted against x_1 for $\bar{R}_0$ equals $0.5\mu m$, $5\mu m$ and $50\mu m$, respectively. The frequency $f_0 = 30kHz$.

Figure 4. The magnitude of (a) the normal component of traction $|\sigma_1|$ and (b) the particle displacement $|u_1|$ are plotted against x_1 for $\bar{R}_0$ equals $0.5\mu m$, $5\mu m$ and $50\mu m$, respectively. The frequency $f_0 = 30kHz$.

Figure 5. The magnitude of (a) the acoustic pressure $|p_1|$ and (b) the particle velocity $|v_1|$ are plotted against x_1 for f_0 equals $19kHz$, $30kHz$ and $41kHz$, respectively. The equilibrium bubble radii $\bar{R}_0 = 5\mu m$.

Figure 6. The magnitude of (a) the normal component of traction $|\sigma_1|$ and (b) the particle displacement $|u_1|$ are plotted against x_1 for f_0 equals $19kHz$, $30kHz$ and $41kHz$, respectively. The equilibrium bubble radii $\bar{R}_0 = 5\mu m$.

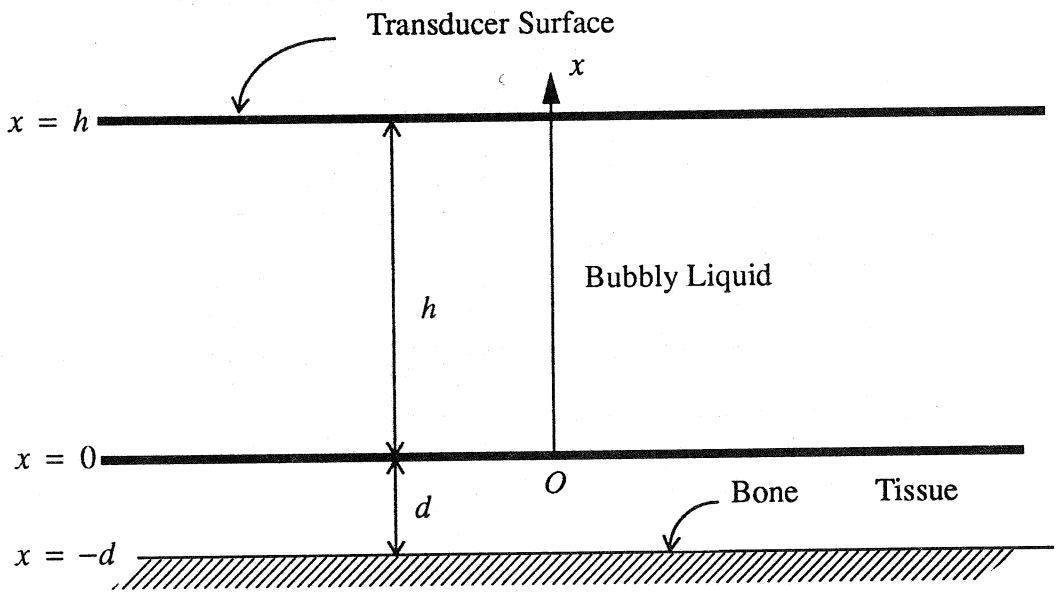

Figure 1

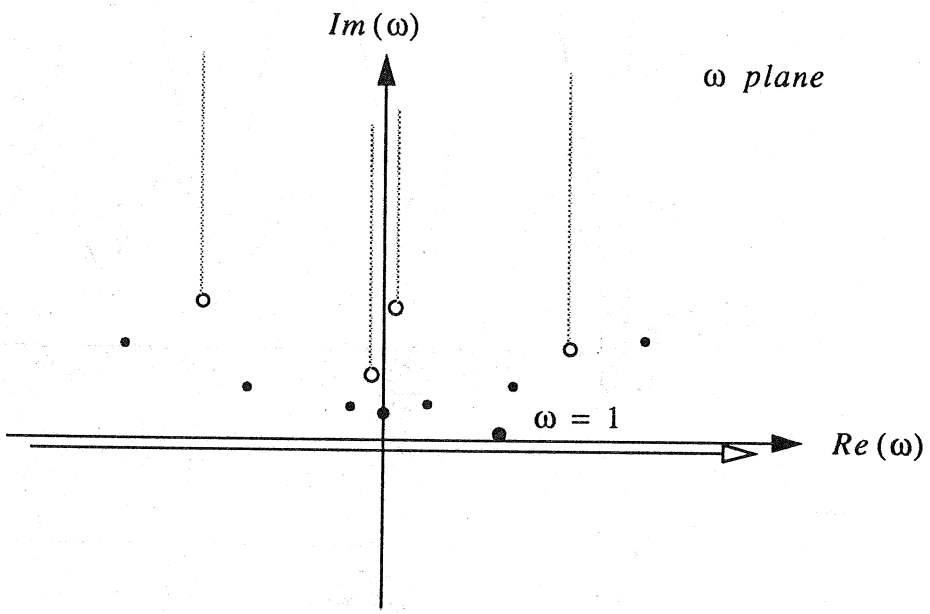

Figure 2

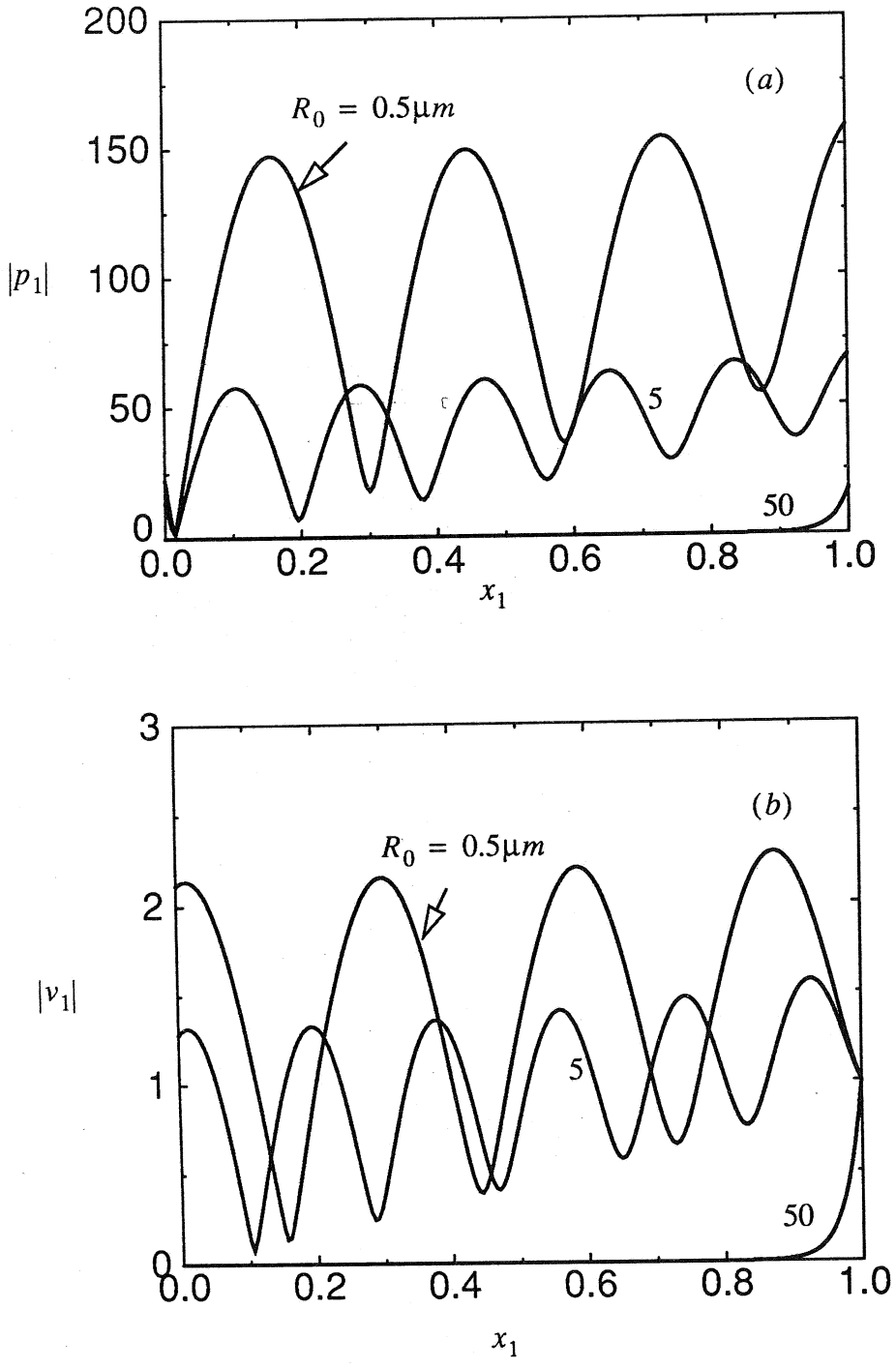
200
150
100
50
0
$|p_1|$
(a)
$R_0 = 0.5\mu m$
5
50
0.0
0.2
0.4
0.6
0.8
1.0
x_1
3
2
1
0
$|v_1|$
(b)
$R_0 = 0.5\mu m$
5
50
0.0
0.2
0.4
0.6
0.8
1.0
x_1

Figure 3

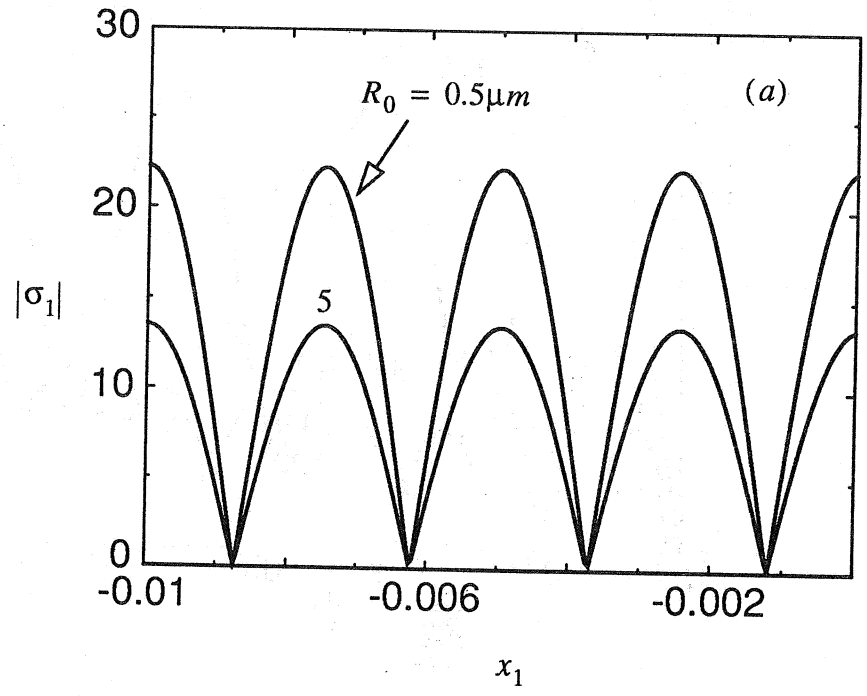
30
20
10
0
$|\sigma_1|$
$R_0 = 0.5\mu m$
(a)
5
-0.01
-0.006
-0.002
x_1

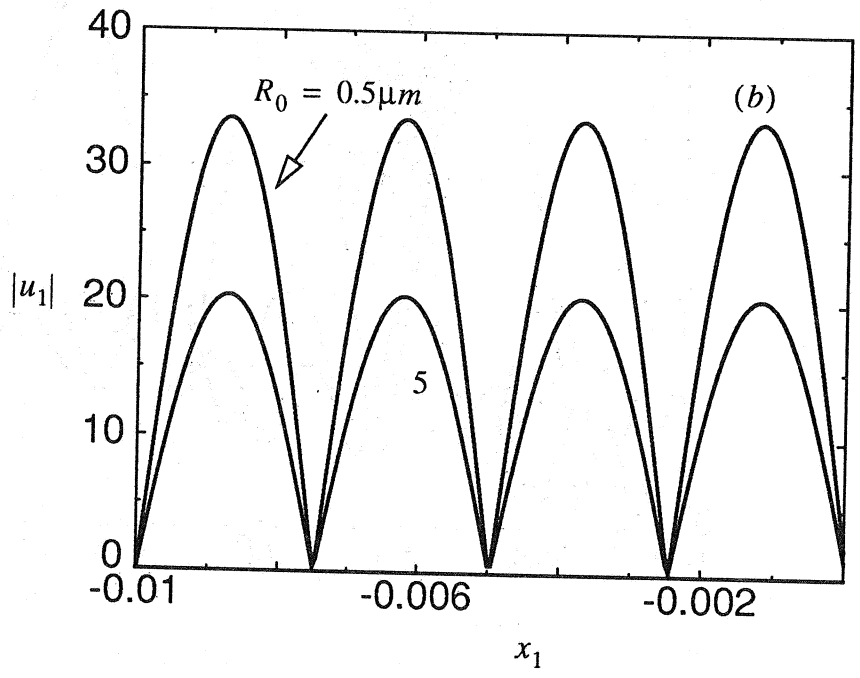
40
30
20
10
0
$|u_1|$
$R_0 = 0.5\mu m$
(b)
5
-0.01
-0.006
-0.002
x_1

Figure 4

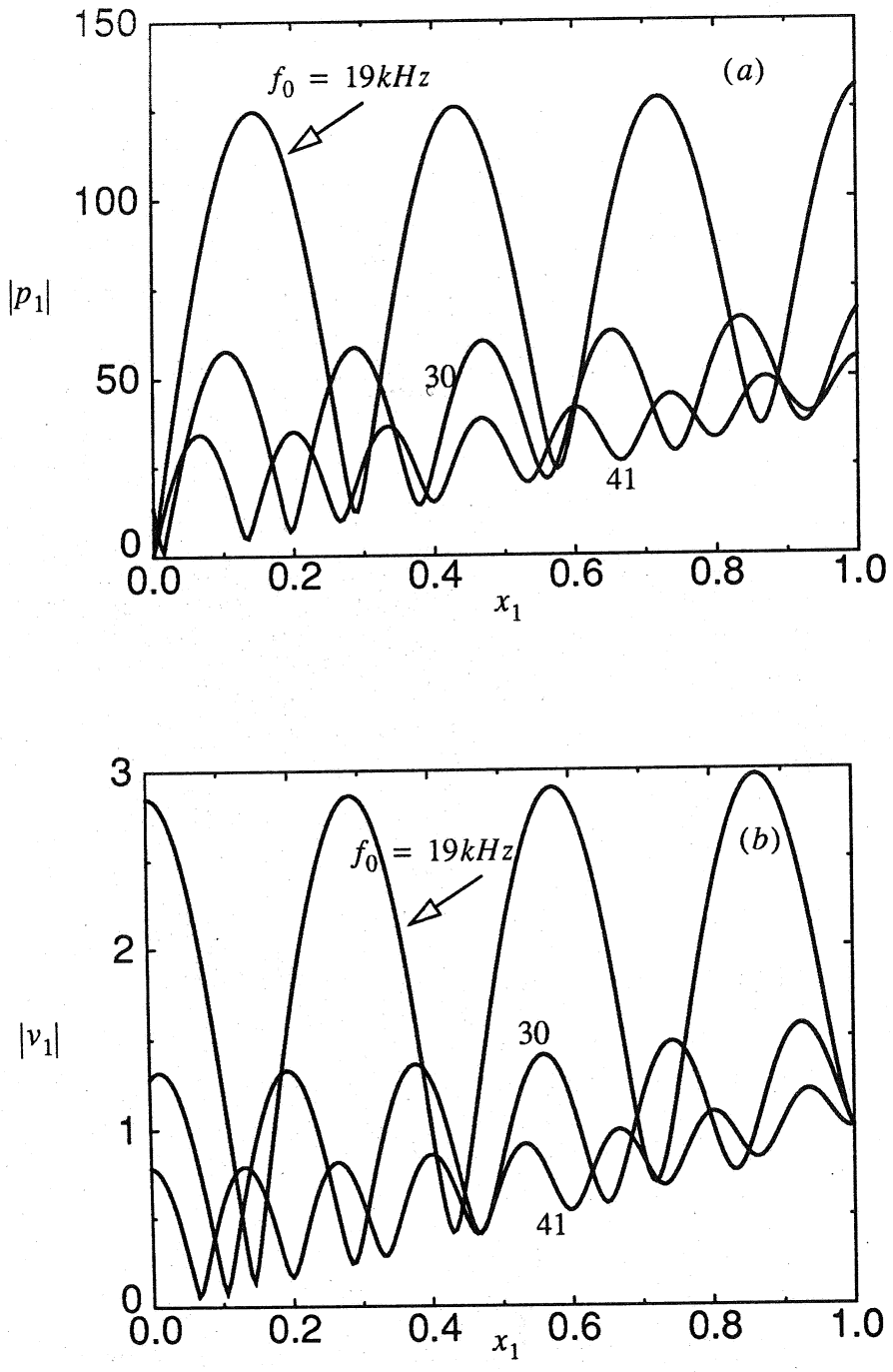
150
100
50
0
$|p_1|$
$f_0 = 19kHz$
(a)
30
41
0.0
0.2
0.4
0.6
0.8
1.0
x_1
3
2
1
0
$|v_1|$
$f_0 = 19kHz$
(b)
30
41
0.0
0.2
0.4
0.6
0.8
1.0
x_1

Figure 5

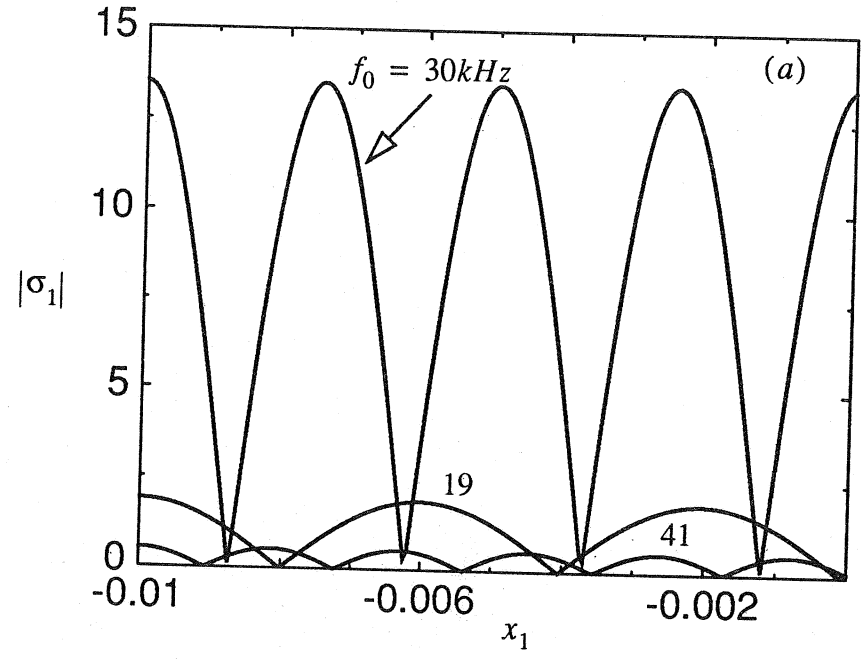
15
10
5
0
$|\sigma_1|$
$f_0 = 30kHz$
(a)
19
41
-0.01
-0.006
-0.002
x_1

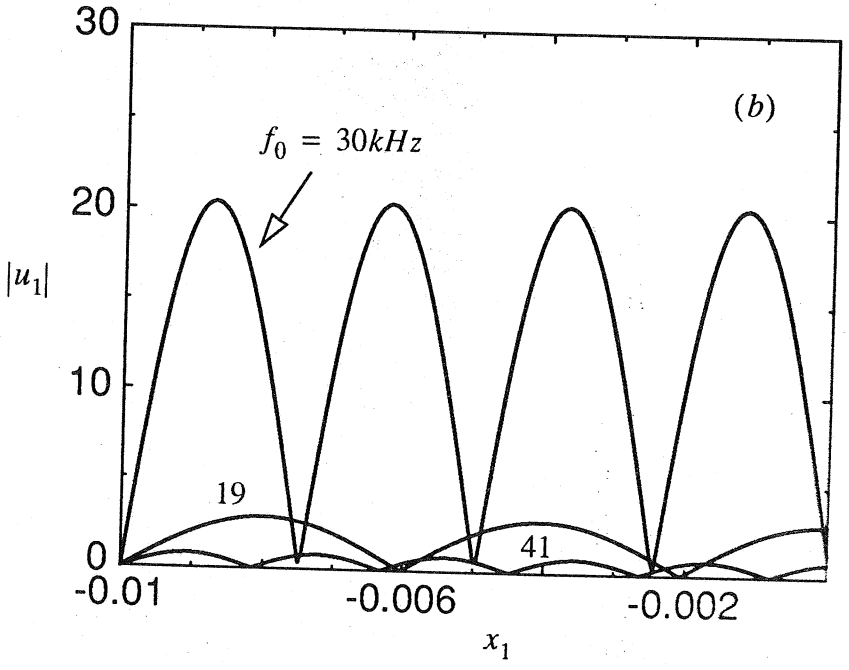
30
20
10
0
$|u_1|$
$f_0 = 30kHz$
(b)
19
41
-0.01
-0.006
-0.002
x_1

Figure 6

List of Recent TAM Reports

No.	*Authors*	*Title*	*Date*
705	Stewart, D. S., and J. B. Bdzil	Asymptotics and multi-scale simulation in a numerical combustion laboratory	Jan. 1993
706	Hsia, K. J., Y.-B. Xin, and L. Lin	Numerical simulation of semi-crystalline nylon 6: Elastic constants of crystalline and amorphous parts	Jan. 1993
707	Hsia, K. J., and J. Q. Huang	Curvature effects on compressive failure strength of long fiber composite laminates	Jan. 1993
708	Jog, C. S., R. B. Haber, and M. P. Bendsøe	Topology design with optimized, self-adaptive materials	Mar. 1993
709	Barkey, M. E., D. F. Socie, and K. J. Hsia	A yield surface approach to the estimation of notch strains for proportional and nonproportional cyclic loading	Apr. 1993
710	Feldsien, T. M., A. D. Friend, G. S. Gehner, T. D. McCoy, K. V. Remmert, D. L. Riedl, P. L. Scheiberle, and J. W. Wu	Thirtieth student symposium on engineering mechanics, J. W. Phillips, coord.	Apr. 1993
711	Weaver, R. L.	Anderson localization in the time domain: Numerical studies of waves in two-dimensional disordered media	Apr. 1993
712	Cherukuri, H. P., and T. G. Shawki	An energy-based localization theory: Part I—Basic framework	Apr. 1993
713	Manring, N. D., and R. E. Johnson	Modeling a variable-displacement pump	June 1993
714	Birnbaum, H. K., and P. Sofronis	Hydrogen-enhanced localized plasticity—A mechanism for hydrogen-related fracture	July 1993
715	Balachandar, S., and M. R. Malik	Inviscid instability of streamwise corner flow	July 1993
716	Sofronis, P.	Linearized hydrogen elasticity	July 1993
717	Nitzsche, V. R., and K. J. Hsia	Modelling of dislocation mobility controlled brittle-to-ductile transition	July 1993
718	Hsia, K. J., and A. S. Argon	Experimental study of the mechanisms of brittle-to-ductile transition of cleavage fracture in silicon single crystals	July 1993
719	Cherukuri, H. P., and T. G. Shawki	An energy-based localization theory: Part II—Effects of the diffusion, inertia and dissipation numbers	Aug. 1993
720	Aref, H., and S. W. Jones	Chaotic motion of a solid through ideal fluid	Aug. 1993
721	Stewart, D. S.	Lectures on detonation physics: Introduction to the theory of detonation shock dynamics	Aug. 1993
722	Lawrence, C. J., and R. Mei	Long-time behavior of the drag on a body in impulsive motion	Sept. 1993
723	Mei, R., J. F. Klausner, and C. J. Lawrence	A note on the history force on a spherical bubble at finite Reynolds number	Sept. 1993
724	Qi, Q., R. E. Johnson, and J. G. Harris	A re-examination of the boundary layer attenuation and acoustic streaming accompanying plane wave propagation in a circular tube	Sept. 1993
725	Turner, J. A., and R. L. Weaver	Radiative transfer of ultrasound	Sept. 1993
726	Yogeswaren, E. K., and J. G. Harris	A model of a confocal ultrasonic inspection system for interfaces	Sept. 1993
727	Yao, J., and D. S. Stewart	On the normal detonation shock velocity–curvature relationship for materials with large activation energy	Sept. 1993
728	Qi, Q.	Attenuated leaky Rayleigh waves	Oct. 1993
729	Sofronis, P., and H. K. Birnbaum	Mechanics of hydrogen–dislocation–impurity interactions: Part I—Increasing shear modulus	Oct. 1993
730	Hsia, K. J., Z. Suo, and W. Yang	Cleavage due to dislocation confinement in layered materials	Oct. 1993
731	Acharya, A., and T. G. Shawki	A second-deformation-gradient theory of plasticity	Oct. 1993
732	Michaleris, P., D. A. Tortorelli, and C. A. Vidal	Tangent operators and design sensitivity formulations for transient nonlinear coupled problems with applications to elasto-plasticity	Nov. 1993
733	Michaleris, P., D. A. Tortorelli, and C. A. Vidal	Analysis and optimization of weakly coupled thermo-elasto-plastic systems with applications to weldment design	Nov. 1993

(continued)

List of Recent TAM Reports (cont'd)

No.	*Authors*	*Title*	*Date*
734	Ford, D. K., and D. S. Stewart	Probabilistic modeling of propellant beds exposed to strong stimulus	Nov. 1993
735	Mei, R., R. J. Adrian, and T. J. Hanratty	Particle dispersion in isotropic turbulence under the influence of non-Stokesian drag and gravitational settling	Nov. 1993
736	Dey, N., D. F. Socie, and K. J. Hsia	Static and cyclic fatigue failure at high temperature in ceramics containing grain boundary viscous phase: Part I—Experiments	Nov. 1993
737	Dey, N., D. F. Socie, and K. J. Hsia	Static and cyclic fatigue failure at high temperature in ceramics containing grain boundary viscous phase: Part II—Modelling	Nov. 1993
738	Turner, J. A., and R. L. Weaver	Radiative transfer and multiple scattering of diffuse ultrasound in polycrystalline media	Nov. 1993
739	Qi, Q., and R. E. Johnson	Resin flows through a porous fiber collection in pultrusion processing	Dec. 1993
740	Weaver, R. L., W. Sachse, and K. Y. Kim	Transient elastic waves in a transversely isotropic plate	Dec. 1993
741	Zhang, Y., and R. L. Weaver	Scattering from a thin random fluid layer	Dec. 1993
742	Weaver, R. L., and W. Sachse	Diffusion of ultrasound in a glass bead slurry	Dec. 1993
743	Sundermeyer, J. N., and R. L. Weaver	On crack identification and characterization in a beam by nonlinear vibration analysis	Dec. 1993
744	Li, L., and N. R. Sottos	Predictions of static displacements in 1–3 piezocomposites	Dec. 1993
745	Jones, S. W.	Chaotic advection and dispersion	Jan. 1994
746	Stewart, D. S., and J. Yao	Critical detonation shock curvature and failure dynamics: Developments in the theory of detonation shock dynamics	Feb. 1994
747	Mei, R., and R. J. Adrian	Effect of Reynolds-number-dependent turbulence structure on the dispersion of fluid and particles	Feb. 1994
748	Liu, Z.-C., R. J. Adrian, and T. J. Hanratty	Reynolds-number similarity of orthogonal decomposition of the outer layer of turbulent wall flow	Feb. 1994
749	Barnhart, D. H., R. J. Adrian, and G. C. Papen	Phase-conjugate holographic system for high-resolution particle image velocimetry	Feb. 1994
750	Qi, Q., W. D. O'Brien Jr., and J. G. Harris	The propagation of ultrasonic waves through a bubbly liquid into tissue: A linear analysis	Mar. 1994